Annuaire de l'Université de Sofia "St. Kliment Ohridski", Faculté de Physique, 97, 2004

ELECTRONIC PROPERTIES OF AlAs/GaAs SUPERLATTICES CONTAINING EMBEDDED GaAs QUANTUM WELLS

KRASSIMIRA GERMANOVA, VESSELIN DONCHEV*,
NIKOLAY SHTINKOV**, STOYAN VLAEV***

Department of Solid State Physics and Microelectronics
**Department of Condensed Matter Physics*
***Department of Engineering Physics, Polytechnic School of Montreal, Montreal, Canada*
****School of Physics, Autonomous University of Zacatecas, Zacatecas, Mexico*

Красимира Германова, Веселин Дончев, Николай Щинков, Стоян Влаев. ЕЛЕКТРОННИ СВОЙСТВА НА СВРЪХ-РЕШЕТКИ ОТ AlAs/GaAs, СЪДЪРЖАЩИ ВЛОЖЕНИ КВАНТОВИ ЯМИ ОТ GaAs

В тази работа се докладват детайлни изследвания на електронната структура на свръхрешетки (СР) от AlAs/GaAs с вложени квантови ями (ВКЯ) от GaAs, проведени чрез теоретични пресмятания и компютърни симулации. Пресмятанията на свързаните състояния на носителите са извършени чрез: 1) метода на обвиващата функция и 2) полуемпиричния sp^3s^* метод на силната връзка, комбиниран с техниката на съшиване на Гриновите функции на интерфейса. Зависимостта на електронната структура от ширината на ВКЯ е пресметната за случая на резки интерфейси. Анализирано е взаимодействието между СР и ВКЯ и неговият ефект върху енергиите и локализацията на свързаните състояния. В детайли е изследван важният и актуален проблем за размиване на интерфейсите и неговото влияние върху електронната структура. За тази цел е разработен прост модел, допускащ дифузен концентрационен профил, отговарящ на малки дифузионни дължини. Моделът е приложен най-напред за регулярна СР с размити интерфейси. Показано е, че СР от тип I може да се трансформира в тип II и са намерени условията за такъв преход. Установено е, че Г–X взаимодействието в проводимата зона на СР бързо намалява при увеличаване интердифузията на материалните компоненти на интерфейсите. Свързаните състояния и енергиите на оптични преходи в СР с ВКЯ са пресметнати в зависимост от степента на размиване на интерфейсите и са сравнени със съответните величини за изолирани КЯ от GaAs. Дадена е разумна интерпретация на резултатите от това сравнение.

Krassimira Germanova, Vesselin Donchev, Nikolay Shtinkov, Stoyan. Vlaev. ELECTRONIC PROPERTIES OF AlAs/GaAs SUPERLATTICES CONTAINING EMBEDDED GaAs QUANTUM WELLS

In this paper, a detailed theoretical and computer simulation study of the electronic structure of AlAs/GaAs semiconductor superlattices (SLs) with GaAs embedded wells (EWs) is carried out.

The calculations of the carrier bound states are performed in frames of: 1) the envelope function approximation and 2) the semi-empirical sp^3s^* tight-binding model combined with the surface Green function matching technique. The dependence of the electronic structure on the EW width is calculated in case of abrupt interfaces. The interaction between the SL and the EW and its effect on the bound state energies and localization are analysed. The important and actual problem of the interface grading effects on the electronic structure is studied in details. To that purpose a simple model is elaborated assuming a diffused concentration profile with small diffusion lengths. The model is applied first to a regular SL with graded interfaces. It is shown that a SL of type I can be transformed in type II and the conditions for such a transformation are determined. Besides, it is found that a rapid decrease of the $\Gamma-X$ interaction in the SL conduction band occurs when the component interdiffusion at the interfaces increases. Further, the bound states and the optical transition energies in SLs containing EWs are calculated as a function of the interface grading degree and compared to the corresponding quantities in the case of single GaAs QWs. A reasonable interpretation of the comparison results is given.

Keywords: AlAs/GaAs superlattices, embedded quantum wells, interface grading, envelope function approximation, tight-binding method, surface Green function matching

PACS numbers: 73.21.-b; 73.21.Cd; 73.21.Fg

1. INTRODUCTION

Quantum heterostructures based on the system GaAs/AlAs have been widely studied and used in practice, due to the good lattice matching between the two materials and the well developed technologies for their fabrication [1–3]. Different GaAs/AlAs electronic and optoelectronic devices with quantum effects are currently commercially available. An increasing tendency in such devices is the implementation of complicated multi-layered nano-systems, containing two or more components interacting with each other. Such systems are for example the superlattices (SLs) with embedded quantum wells (QWs). They represent a SL, in which one or more of the QWs are wider or narrower than the others.

Short-period AlAs/GaAs SLs containing embedded wells (EWs) have recently received considerable interest [4–18]. From one hand they show intriguing physical properties often different from those of single QWs and unperturbed SLs [10–13]. From the other hand these structures have many advantages in comparison with single GaAs QWs with homogeneous AlGaAs alloy barriers: i) The use of SLs as prelayers suppress the defect diffusion from the substrate to the EW and relieves the strain caused by the small lattice mismatch between GaAs and AlAs [7, 8]. This improves the device parameters. For example in GaAs quantum well lasers with short-period AlAs/GaAs SL barrier regions the optical scattering losses and the barrier non-radiative recombination are essentially reduced [7]; ii) The existence of SL barriers enables a better control of the system structural parameters. This is very important for the growth of ultrathin layers on patterned substrates used in the fabrication of quantum wires [9]; iii) SLs with EWs are suitable for studying the carrier transport perpendicular to the layers [18]. All these facts show that the structures described are very interesting for both the fabrication of advanced optoelectronic devices and the fundamental physics.

The electronic structure and the optical properties of AlAs/GaAs SLs with

EWs have been studied in various papers assuming rectangular potential, i.e. abrupt interfaces. However it is known that, due to the complicated nature of the growth mechanisms, the chemical composition of the interface is a function of the space coordinate in both lateral (in the plane of the interface) and vertical (along the growth axis) direction. As a result the interface potential has a non-abrupt profile, which influences significantly the electronic structure, electrical and optical properties of the QWs and the SLs. These effects can influence the device parameters and/or lead to completely new effects in the device. Therefore the study of the effect of graded interfaces on the properties of the heterostructures is a very important question from both fundamental and practical point of view. Up to now this effect has been partially investigated only in some simple heterostructures [19–21].

In this paper we present a comprehensive theoretical and numerical simulation study of the electronic structure of short-period AlAs/GaAs SLs containing one EW with abrupt and graded interfaces. The calculations are performed by means of two methods: the envelope function approximation (EFA) and the semi-empirical sp^3s^* spin-dependent tight-binding model combined with the surface Green function matching (SGFM) technique. The case of abrupt interfaces is considered in Section 2, where the interaction between the two components of the system—SL and EW is emphasized. Section 3 deals with graded interfaces. It starts with a simple model of the interface grading based on a diffused concentration profile with small diffusion lengths. The model is applied first to $(AlAs)_m/(GaAs)_n$ SLs with graded interfaces. It is studied how the diffusion can result in i) a transformation of the SL from type I to type II, and ii) a strong decrease of the $\Gamma - X$ interaction in the SL conduction band. Further, the electronic structure and optical transition energies in SLs containing EWs are calculated as a function of the degree of interface grading and compared to the same quantities in the case of single GaAs QWs.

2. ELECTRONIC STRUCTURE CALCULATIONS OF SUPERLATTICES CONTAINIG EMBEDDED QUANTUM WELLS WITH ABRUPT INTERFACES

2.1. NANOSTRUCTURES

The structures considered consist of a finite $(AlAs)_4/(GaAs)_8$ SL, grown in [001] direction and surrounded by semi-infinite $Al_{0.33}Ga_{0.67}As$ buffer layers. The width of the central well of the SL varies from 2 to 50 monolayers (ML). On each side of this well there are 5.5 SL periods (five wells and six barriers).

2.2. ENVELOPE FUNCTION APPROXIMATION (EFA)

The calculations are made for the Γ point of the two-dimensional (2D) Brillouin zone using a simple one-band envelope-function model [3]. The envelope-function equation is solved numerically by the finite difference method, choosing the discretisation step small enough to achieve accuracy better than 0.5 meV over the whole energy range of interest. The effective masses m^* of electrons, heavy holes (HH) and light holes (LH) are 0.0665, 0.327 and 0.09 in GaAs and 0.15, 0.478 and 0.208 for electrons, HH and LH in AlAs, respectively [22]. For the effective masses in $Al_xGa_{1-x}As$ linear interpolations between those in AlAs and GaAs are employed. The bandgap of $Al_xGa_{1-x}As$ at the Γ point is expressed as [22]: $E_G(x) = 1.519 + 1.087x + 0.438x^2$. The conduction to valence band-offset ratio is 66/34 [23]. The zero energy is at the bottom of GaAs conduction band for electrons and at the top of GaAs valence band for holes. The AlAs and GaAs parameters used in the calculations are given in Table 1.

The energies of the bound states for electrons, HH and LH are shown on Fig. 1 for EW widths from 2 to 50 ML. On the figure are clearly seen the energy spectra of both components of the system—EW (localized states) and SL (minibands). The energies of the EW states reveal a strong dependence on the EW width, while the SL state energies remain constant.

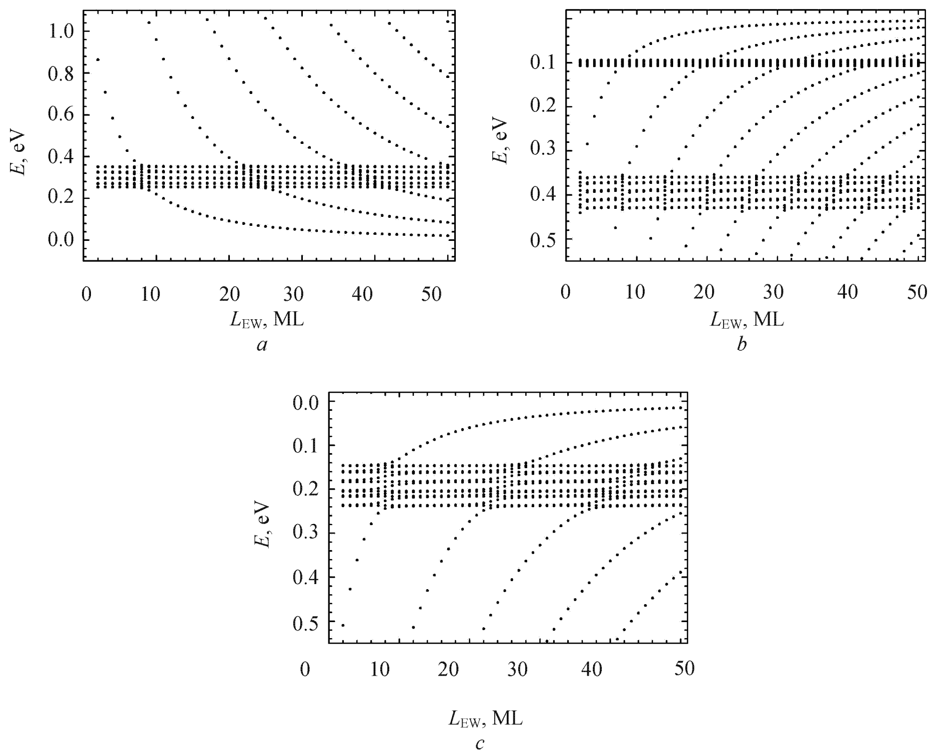

Fig. 1. Energies of bound states for: *a*) electrons, *b*) heavy holes, and *c*) light holes versus the EW width, calculated by means of the EFA

Table 1. Parameters of AlAs and GaAs used in the calculations by the envelope function approximation

Parameter	Symbol	AlAs	GaAs	Reference
Electron effective mass in Γ	$m_e^*(\Gamma)/m_0$	0.150	0.0665	[24]
Electron longitudinal Effective mass in X	$m_l^*(\mathrm{X})/m_0$	1.1	1.8	[22]
	γ_1	3.45	7.10	[25] for AlAs
Luttinger parameters	γ_2	0.68	2.02	[26] for GaAs
	γ_3	1.29	2.90	
Bandgap in Γ	$E_G(\Gamma)$, eV	3.130	1.51914	[22]
Bandgap in X	$E_G(\mathrm{X})$, eV	2.23	2.10	[22]

There are ranges of EW widths where all the EW states have energies far from the SL minibands (e.g., 12 to 18 ML for electrons). In these ranges the EW states are very close in energy to the localized states of a single rectangular GaAs QW of the same width with AlAs barriers. The difference between the corresponding energy levels does not exceed 1 meV. The EW breaks the SL into two identical subsets and the SL states in the miniband are coupled in pairs, corresponding to symmetric and antisymmetric combinations between the states of the subsets. The calculation of the wave functions in these regions shows that the EW and the SL states are localized in the corresponding parts of the structure and no spatial penetration from EW into SL (or vice versa) is observed. (Fig. 2). Thus, in these ranges of EW widths the system could be considered as a combination of non-interacting components: EW and SL.

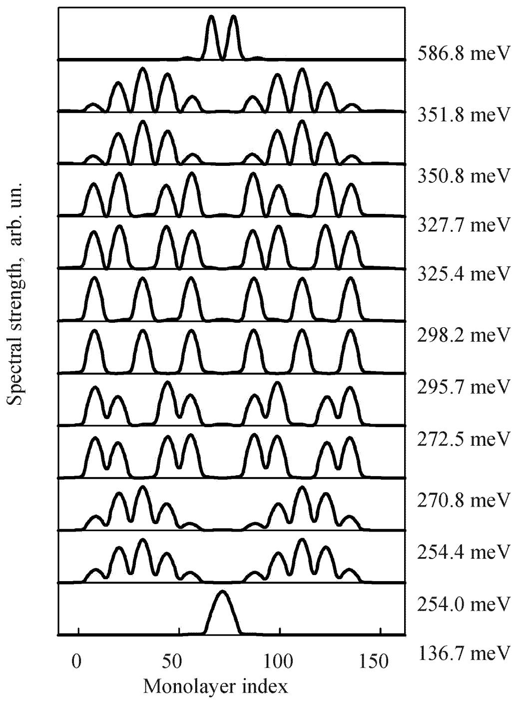

Fig. 2. Spatial distribution of the states ($|\Psi|^2$) of the EW and the SL for an EW width of 15 ML, calculated by means of the EFA. ML index 1 corresponds to the first ML from the SL

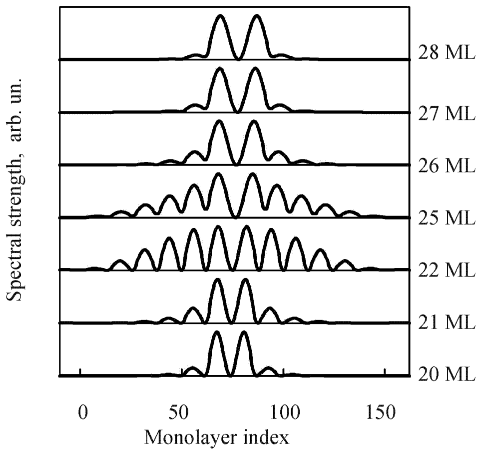

Fig. 3. Spatial distribution of the states ($|\Psi|^2$) of the second EW electron state for selected EW widths (between 20 and 28 ML), for which this state has an energy close to the SL miniband. The calculations are performed by means of the EFA. ML index 1 corresponds to the first ML from the SL

A particular interest represent the EW widths for which some of the EW states has an energy close to the SL miniband, because in these regions an interaction between the EW and the SL is observed. We have calculated the wave functions of the second EW electron state for selected EW widths (between 20 and 28 ML), for which this state has energy close to the SL miniband (250–350 meV). The results are shown on Fig. 3. The energy difference between the EW level and the miniband changes with increasing the EW width. When it becomes about 50–60 meV, the EW state is delocalized only in the first-neighbour wells of the SL. The delocalization of this state towards the SL increases if its energy gets closer to the miniband. For states closer than 10 meV to theminiband (EW width between 22 and 25 ML) the mixing between the EW and the SL states is so strong that they become localized equally in the EW and the SL.

When the EW state is degenerated with the SL miniband, it interacts strongly with the SL states. As a result the total number of states in the miniband becomes 11. Such is the case of EW width equal to 24 ML, where the second EW state lies in the SL miniband. The energies and localizations of these 11 states are displayed in Fig. 4. As seen on the figure, none of the states is localized only in the EW. This implies, that the interaction provokes a delocalization of the EW state towards the SL and thus it becomes undistinguishable from the SL states. On the other hand, the latter are also influenced by the interaction. As the second EW state is odd (antisymmetric with respect to the EW centre) it couples only with the antisymmetric SL states, which results in six interacting states. The coupling changes their energies and spatial localizations. The antisymmetric SL states penetrate in the EW, where they reveal two maxima and shift in energy, thus disturbing the couples of states depicted above. The coupling is better pronounced for the states with lower energies, because the EW state is expected to be in the lower part of the SL miniband. The other five even (symmetric) SL states remain unchanged.

The same effect is observed for the third EW state (EW widths from 36 to

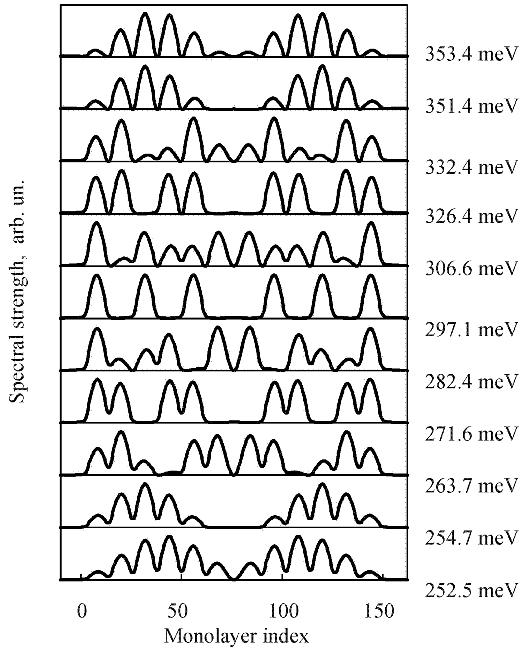

Fig. 4. Spatial distribution of the SL miniband states ($|\Psi|^2$) for EW width of 24 ML. The second EW state lies inside the miniband and is undistinguishable from the SL states. The calculations are made by means of the EFA. ML index 1 corresponds to the first ML from the SL

42 ML). The only difference is that being an even state, it interacts only with the even SL states. For EW widths around 36 ML the interaction is stronger with the SL states near the upper miniband edge, while for 42 ML it is stronger near the lower edge.

The valence band reveals similar behaviour. The EFA model used does not take into account the interaction between LH and HH in the Γ point of the Brillouin zone.

2.3. EMPIRICAL TIGHT-BINDING APPROACH (ETB)

The calculations are made using the semi-empirical sp^3s^* spin-dependent tight-binding Hamiltonian, the virtual crystal approximation, and the surface Green function matching technique. The Green functions of the wells and the barriers are matched simultaneously at all the interfaces using the formulae given in [27], which makes calculations faster. The tight-binding parameters for AlAs and GaAs are taken from [28] and modified according to [29] in order to take into account the spin-orbit coupling. In the energy reference used here, $E_v(\text{AlAs}) = 0$, $E_c(\text{AlAs}) = 2.27$ eV, $E_v(\text{GaAs}) = 0.548$ eV, and $E_c(\text{GaAs}) = 2.10$ eV. For the valence and conduction band edges energies of $Al_{0.33}Ga_{0.67}As$ we obtain 0.37 eV and 2.41 eV, respectively. The band-offset ratio (66/34) is the same as in the EFA calculations. The obtained bound states are described with respect to their energy, spatial distribution and orbital character.

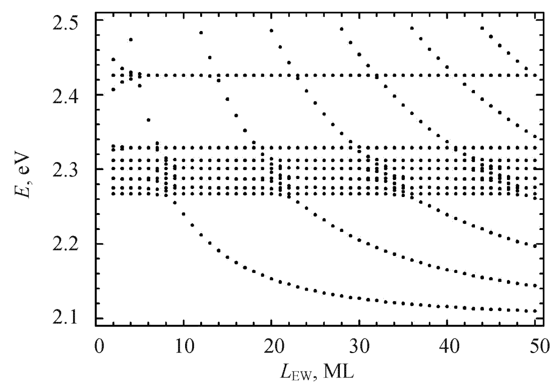

Fig. 5. Energies of conduction band bound states for EW widths from 2 to 50 ML, calculated by means of the empirical tight-binding method

The energies of the electron and hole states are calculated for the Γ point of the 2D Brillouin zone in the energy ranges from 0.3 to 0.548 eV for the valence and from 2.1 to 2.5 eV for the conduction bands, with an energy resolution of 0.001 eV.

The energies of the conduction band bound states are plotted on Fig. 5 as a function of the EW width. On the figure are clearly seen the states originating from the SL, whose energies are practically independent of the EW width, as well as states originating from the EW, with energies decreasing as the EW gets wider.

The EW states are spatially localized predominantly in the EW, and have s orbital character. Their energies are the same as those of the corresponding states in a single GaAs/AlAs quantum well, except in the cases, when they are close to a SL state. The SL states can be divided in two groups. In the first one are the states localized in the SL wells, forming a miniband with energies from 2.262 eV to 2.313 eV. These states also have s orbital character and originate from the Γ point of the GaAs conduction band. As in Sect. 2.2. the EW divides the SL into two parts. As a result the ten states in the miniband group into five couples with close energies. Their wavefunctions are either symmetric or antisymmetric combinations of the state wavefunctions of the two sets of states.

In the second group are the states localized in the SL barriers with energies 2.327 eV and 2.424 eV. For them the main contribution to the density of states is from the p_z orbital, which implies that they originate from the Γ projection of the X_z minima of the AlAs conduction band. They are very strongly localized and the interaction between them becomes visible for EW widths below 7 ML, where an energy splitting of the two states from the central barriers is observed. The states at 2.424 eV are above the $Al_{0.33}Ga_{0.67}As$ conduction band edge, which explains their nonzero spectral strength in the buffer layers. Both types of SL states do not penetrate in the EW when the EW states energies are away from the SL minibands.

When an EW state has energy close to or inside the SL miniband it interacts with the SL states. This interaction is similar to the one described in Sect. 2.2.

The calculated energies and spatial distributions of the electron states for an EW width of 35 ML are displayed in Fig. 6. For this structure the third EW bound state energy lies in the SL miniband, as can be seen from Fig. 5, and the total number of states in the miniband is 11. The calculations are made using a better energy resolution of 0.1 meV in order to separate the different states. Fig. 6 shows that, as in the former Sect. 2.2., interact only states with the same parity—even (symmetric) in the case considered. The coupling changes the localization and the energies of the interacting states. In particular the symmetric SL states penetrate in the EW revealing three maxima and shift in energy, thus disturbing the couples of states depicted above. The asymmetric SL states do not interact with the EW state.

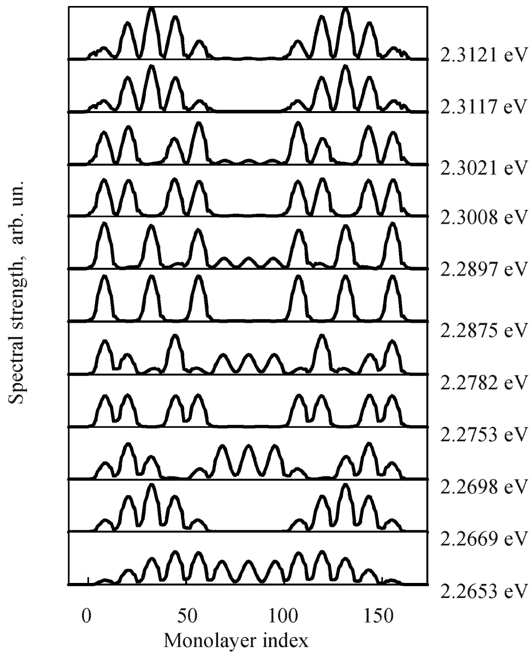

Fig. 6. Spatial distribution of the states ($|\Psi|^2$) in the first electron miniband of the SL for an EW width of 35 ML, calculated by means of the ETB method. ML index 1 corresponds to the first ML from the SL

With increasing (decreasing) the EW width above 36 ML (below 32 ML) the described interaction weakens. The third EW state gradually emerges from the bottom (top) of the miniband and its wavefunction becomes localized in the EW.

Similar interaction between states of equal parity is observed when the first, second and fourth EW states are close to or inside the SL miniband. This happens for EW widths of 7–9, 19–23 and 42–50 ML, respectively.

Another interesting result is the interaction between the EW states with the second group of SL states, which have different orbital characters. The interaction occurs when the states are very close in energy. The coupled states have mixed s-p_z orbital character and are localized in the EW and the nearest AlAs barriers.

The situation in the valence band is more complicated. The energies of its bound states are shown on Fig. 7. As in the conduction band, there are EW and SL states, which can be divided into three groups with respect to their orbital character: HH states (the contribution of the p_z orbital is nearly zero), LH states (the main contribution is from the p_z orbital), and mixed states. The mixing takes place when two states are close in energy, and manifests itself in energy shifts, changes in the localization and changes in the orbital character of the interacting states.

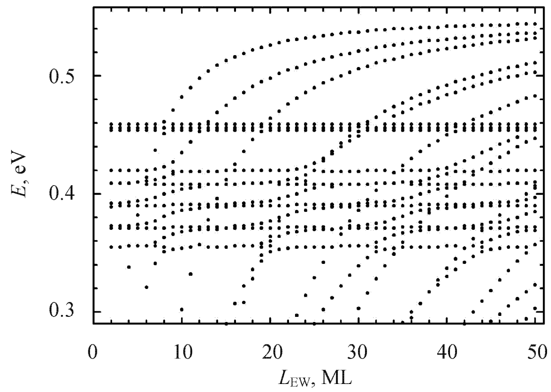

Fig. 7. Energies of valence band bound states for EW widths from 2 to 50 ML, calculated by means of the ETB method

It is worth to be noted that the ETB method describes better the electronic properties of complicated structures than the EFA. Many interesting features of the band structure, such as HH–LH mixing at the Γ point of the Brillouin zone, the presence of SL states with AlAs localization and their interaction with the EW electron states, can be obtained only by more sophisticated methods like the tight-binding one.

The EW can be considered as an effective imperfection in the regular SL. The coupling-decoupling of an EW state with (from) the SL miniband states depends on the EW width, i.e. on the strength of the perturbation. This effect is in principle similar to the formation of localized electronic states in a bulk crystal containing different types of defects [30]. We believe our study could give an insight into this interesting problem, which needs further investigations. As far as we know the dependence of the electronic structure on the EW width has not been studied in details until now. The analysis of the interaction between EW and SL is important for a better understanding of the optical properties of complicated nanoheterostructures used in advanced devices.

3. ELECTRONIC STRUCTURE OF NANOHETEROSTRUCTURES WITH GRADED INTERFACES

3.1. MODELLING OF THE INTERFACE GRADING

In studying the electronic structure and the optical properties of semiconductor nanoheterostructures usually perfect interfaces, i.e., abrupt transitions between the different materials have been considered. The real interfaces however have substantial roughness on an atomic scale [31–34]. Different sources of this interface disorder have been suggested, such as surface segregation of Ga atoms and Ga–Al interdiffusion by direct exchange of atoms or via interactions with intrinsic defects [31, 32, 34–36]. These effects lead to an effective broadening of the interfaces and influence the electronic and optical properties of the entire structure and thus of the devices based on it.

In this section we present the results of our theoretical investigations of GaAs based nanostructures with graded interfaces. The interface grading is taken into account by averaging the lateral disorder over the layer planes and assuming a non-abrupt potential in the growth direction. In our model this potential is effectively represented by a diffusion potential profile, corresponding to diffusion lengths of about several ML. This profile is determined by the Al concentration profile. The diffusion length is used as a parameter characterizing the degree of interface broadening. The use of such model is justified, because it explains reasonably well photoluminescence experimental data [14].

The concentration profile $C(z,t)$ of the structures homogeneous in the (x,y) plane, is obtained from the one-dimensional diffusion equation. For GaAs/AlGaAs structures we assume a concentration independent diffusion coefficient, D. Than the diffusion equation becomes:

$$\frac{\partial C(z,t)}{\partial t} = D\frac{\partial^2 C(z,t)}{\partial z^2} \tag{1}$$

The general solution for a structure with initially rectangular concentration profile, i.e. which consists of N initially homogeneous layers is [20]:

$$C(z) = C_0 + \frac{1}{2}\sum_{n=1}^{N}(C_{n-1} - C_n)\, erf\left[\frac{(z_n - z)}{L_D}\right] \tag{2}$$

Here C_i is the initial Al concentration in the i^{th} layer ($i = 1,\ldots,N$), z_j is the coordinate of the j^{th} interface (between the j^{th} and $(j+1)^{\text{th}}$ layers, $j = 1,\ldots,N$) and L_D is the diffusion length. Thus, given the initial concentrations C_i we can calculate the concentration profile along the structure for any value of L_D. As mentioned above, L_D plays here the role of a parameter characterizing the degree of interface grading. However equation (2) can be readily used for any diffused structures where the value of L_D is calculated from the conventional formula $L_D = 2(D\,t)^{1/2}$, knowing the values of the diffusion coefficient and the time of diffusion, t.

3.2. REGULAR (NON-PERTURBED) SUPERLATTICES

3.2.1. Energies and widths of the minibands

We have calculated the lowest electron, HH and LH minibands of an $(AlAs)_4/(GaAs)_8$ SL with 10 periods. The concentration profile of the SL for different diffusion lengths is given on Fig. 8. The calculations are performed in frames of

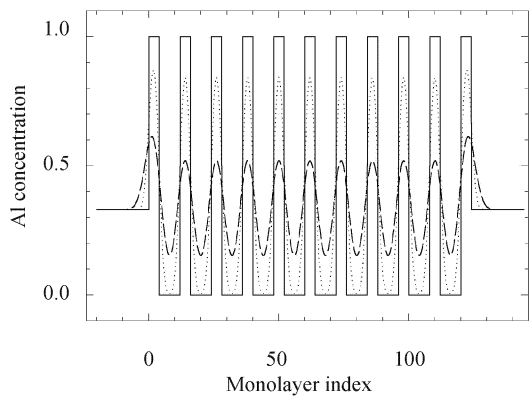

Fig. 8. Concentration profiles in the SL for nondiffused (solid line) and diffused structure with diffusion length $L_D = 2$ ML (dotted curve) and $L_D = 4$ ML (dashed curve)

the EFA for the Γ point of the 2D Brillouin zone. The behaviour of the minibands with the diffusion length is studied in the range from$L_D = 0$ to $L_D = 4$ ML. The results are shown on Fig. 9.

Two effects can be seen when L_D increases: i) the energies of the miniband states increase; ii) the minibands get wider. The first effect is due to the fact that with increasing L_D the miniband states demonstrate similar behaviour as those of a single QW [20], because they originate from the SL wells. The second effect is connected with the fact that the SL miniband width is determined by the coupling between the neighbouring wells of the SL. Because with increasing the L_D the SL barriers get lower (and thinner), the coupling between the wells gets stronger, and so the miniband widen.

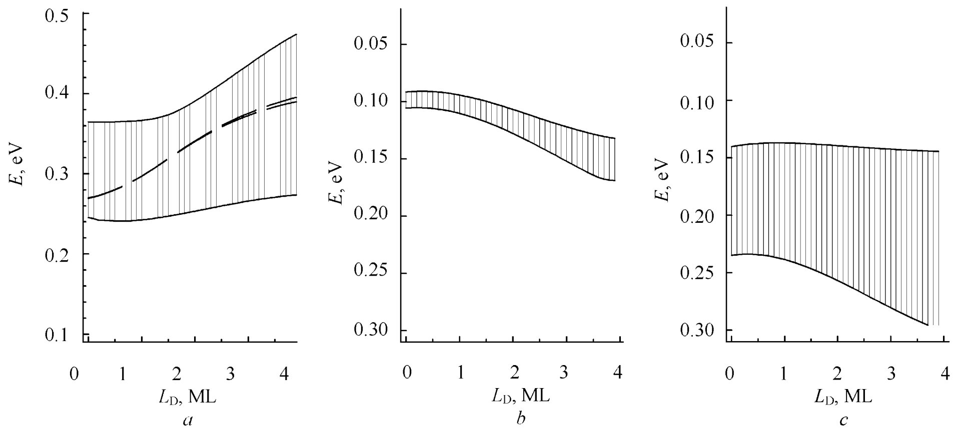

Fig. 9. Energies of the minibands in $(AlAs)_4/(GaAs)_8$ SL versus L_D for: *a*) electrons, *b*) heavy holes, and *c*) light holes, calculated by means of the EFA. The energies of the conduction band bound states originating from the X points of the Brillouin zone are shown with dashed curves (*a*)

In order to obtain a more detailed picture of the electronic structure of the SL we have taken into account the contribution of the conduction band X minima. They give rise to another set of SL states (labelled X_Z miniband) at the centre of the 2D Brillouin zone of the heterostructure, spatially localized in the AlAs layers. The energies of these states are calculated using the same one-band model and the parameters given in Table 1. The $\Gamma-X$ coupling is neglected. The obtained values are also plotted in Fig. 9. The X_Z miniband is substantially narrower than the Γ miniband due to the stronger localization of the X-electrons in the AlAs layers. It shows generally the same behaviour as the Γ miniband, but the energies of the states increase faster withL_D. This is due to the small width of the AlAs layers (4 ML), which results in a fast decrease of the Al concentration even at small diffusion lengths.

The one-band EFA models can not take into account the interaction between the Γ and X states of the conduction band. As we have seen in Sect. 2, this interaction changes the energies, space distributions and character of the states. That is why in studying these states in the next two sections we have used the ETB method.

3.2.2. Interdiffusion induced change of the SL type

$(AlAs)_m/(GaAs)_n$ superlattices with abrupt interfaces are known to undergo a type I (direct) to type II (indirect) transition above $m = 8$ MLs [37] where the conduction band minimum of the system changes from GaAs Γ-like to AlAs X-like. This transition, however, can be obtained not only by changing the numbers of AlAs and GaAs MLs in the SL. The component interdiffusion across the interfaces changes the electronic structure of the system and may result in a crossover of the Γ and X states energies. This mechanism is responsible for the interdiffusion-induced transition from type I to type II SL, which should be observable experimentally as a quenching of the photoluminescence intensity. Recently such a transition has been reported for single AlAs/GaAs quantum wells [36]. We have studied for the first time this transition in $(\mathrm{AlAs})_m/(\mathrm{GaAs})_n$ SLs.

The electronic structure of the diffused SL is calculated in frames of the ETB model with the help of the SGFM formalism and using an algorithm for calculating the Green function of a non-homogeneous slab [38]. The calculations are made at the Γ point of the SL's Brillouin zone. We have investigated infinite $(\mathrm{AlAs})_m/(\mathrm{GaAs})_n$ SLs with $m = 6$ to 22 and $n = 9$ to 15. The change of the energies of the first Γ and X states in an $(\mathrm{AlAs})_8/(\mathrm{GaAs})_{10}$ SL with the diffusion length is shown on Fig. 10. It is seen from Fig. 10 that with increasing L_D, the energy of the X state increases more slowly than the energy of the Γ state, i. e., the X state is less sensitive to the diffusion than the Γ state. Two reasons are responsible for this effect: i) the longitudinal effective mass in the X point of AlAs is greater than the electron effective mass in the Γ point of GaAs (the heavier particle is less sensitive to the change of the well potential); and ii) the change of the potential for X electrons is actually smaller, because the quantum wells formed by the bulk X valley are shallower.

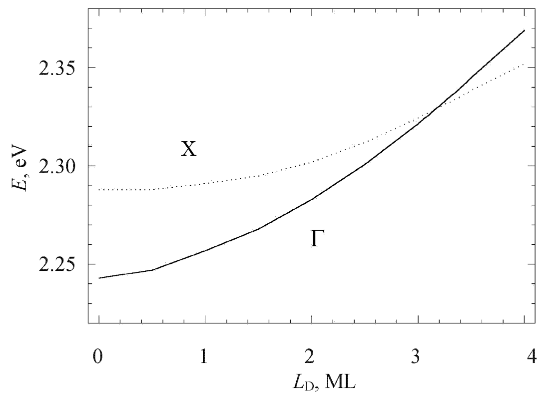

Fig. 10. Dependence of the energies of the first Γ and X conduction band states on the diffusion length L_D in $(\mathrm{AlAs})_8/(\mathrm{GaAs})_{10}$ SL

As a result of this effect, a SL of type I (direct) turns into a SL of type II (indirect) at a certain critical value of the diffusion length L_{Dcr}, above which the lowest energy electron state is of X character. When L_D is infinite, the SL turns into bulk $\mathrm{Al}_x\mathrm{Ga}_{1-x}\mathrm{As}$ with Al concentration x equal to the mean Al content in the SL, i.e., $x = m/(m+n)$. This material has an indirect band structure above the critical concentration $x_\mathrm{c} = 0.43$ [22], therefore the direct-to-indirect transition can take place where the following condition is satisfied:

$$\frac{m}{m+n} > x_c. \tag{3}$$

The obtained values for L_{Dcr} in the investigated SL are given in Table 2. It is seen that at constant m, L_{Dcr} increases with n, which is due to the fact that when the GaAs layers are wider, the necessary increase of the potential for the Γ electrons is obtained at higher diffusion lengths. On the other hand, at constant n, L_{Dcr} decreases with increasing m, approaching constant. When m increases, the energy of the X states converges to the energy of the X minimum in bulk AlAs. For sufficiently wide AlAs layers they are practically not affected by interdiffusion and are acting as an infinite source of Al, diffusing in the GaAs layers through the interfaces. In this case the change of the Al concentration profile in the SL does not depend on m, therefore L_{Dcr} approaches constant.

For SL with close energies of the Γ and X states ($n = 9$), the value of L_{Dcr} is very small (below 1 ML). As shown in the literature [15, 31], such diffusion lengths can be obtained during the growth process. On the other hand, the essential changes of the electronic and the optical properties of the SL due to the observed direct-to-indirect transition give new opportunities for design and fabrication of novel structures and devices. The small values of L_{Dcr} required for the transition can be obtained e.g. by ion implantation or laser annealing [39], thus allowing modulating the SL properties in the lateral direction.

Table 2. Critical diffusion length L_{Dcr} (in ML) for $(AlAs)_m/(GaAs)_n$ SLs. The SLs, for which the condition Eq. (3) is not satisfied, are denoted with "×".

$m\backslash n$	9	10	11	12	13	14	15
6	4.00	×	×	×	×	×	×
7	2.30	4.35	×	×	×	×	×
8	1.58	3.15	4.85	6.70	×	×	×
9	1.30	2.50	3.93	5.45	7.08	×	×
10	1.15	2.20	3.35	4.70	6.08	7.60	9.40
11	1.10	2.08	3.05	4.10	5.40	6.75	8.18
12	1.00	2.00	2.85	3.80	4.90	6.10	7.40
13	0.90	1.95	2.75	3.60	4.50	5.60	6.80
14	0.75	1.85	2.70	3.50	4.30	5.27	6.35
15	0.75	1.80	2.65	3.40	4.20	5.00	6.00
16	0.75	1.70	2.60	3.35	4.10	4.85	5.70
17	0.65	1.68	2.50	3.30	4.00	4.74	5.52
18	0.63	1.68	2.50	3.25	3.95	4.65	5.40
19	0.55	1.65	2.46	3.20	3.90	4.60	5.30
20	0.55	1.60	2.43	3.15	3.85	4.53	5.20
21	0.55	1.58	2.40	3.13	3.85	4.47	5.15
22	0.53	1.55	2.40	3.10	3.80	4.41	5.10

3.2.3. Γ−X coupling in diffused AlAs/GaAs superlattices

The quantum mechanical mixing between bulk Γ and X_z states, introduced by the SL potential in $(AlAs)_m/(GaAs)_n$ superlattices is of great importance for the electronic and optical properties of the SL [40]. This mixing is strongly affected by the interface imperfections, however there have been almost no theoretical investigations of this influence until now. The $\Gamma-X_z$ coupling has been calculated for a single segregated interface [41] and for the case of random exchange of atoms between the adjacent atomic planes at the interface [42]. We investigate for the first time the effect of interdiffusion on the $\Gamma-X_z$ coupling in (001) $(AlAs)_m/(GaAs)_n$ SLs.

The electronic structure of the diffused SL is calculated using the ETB model, as in Sect. 3.2.2. The Γ−X coupling matrix element $V_{\Gamma X}$ is calculated as one half of the minimum anticrossing gap between the first Γ and X_z SL state's dispersion curves in (100) direction $k = (k_x, 0, 0)$.

It is known that in SLs with abrupt interfaces the coupling between the first Γ and X_z states takes place when the number m of AlAs monolayers is even [43].

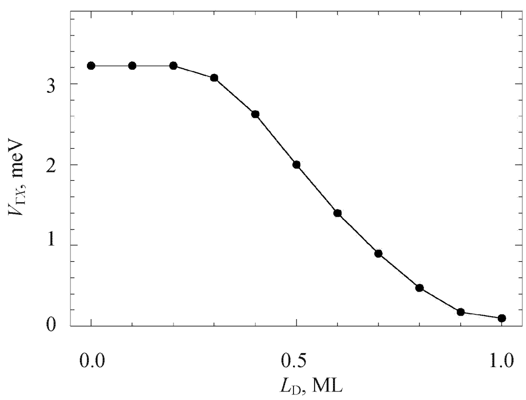

Fig. 11. Dependence of the Γ–X coupling matrix element $V_{\Gamma X}$ on the diffusion length L_D in $(AlAs)_6/(GaAs)_{14}$ superlattice

In agreement with this we obtain $V_{\Gamma X} = 0$ for odd values of m, for abrupt as well as for diffused interfaces. When m is even, however, the coupling matrix element is nonzero for abrupt interfaces and depends strongly on the interdiffusion at the interfaces. This dependence is shown on Fig.11. It is seen from the figure that $V_{\Gamma X}$ is constant up to $L_D = 0.2$ ML and decreases rapidly with further increase of the diffusion length. The coupling practically disappears for L_D greater than 1 ML (2.83 Å). It is very likely to have such degree of intermixing in AlAs/GaAs heterostructures, as shown in many investigations of the AlGaAs/GaAs interface quality [15, 31].

The obtained values of $V_{\Gamma X}$ are between 3.2 meV for abrupt interfaces and 0 for $L_D > 1$ ML. The experimental value for AlAs/GaAs SLs with a period of 20 ML is 2 meV [40], which corresponds to a diffusion length of 0.65 ML. Other theoretical calculations [41, 42] also give similar values for $V_{\Gamma X}$, however we should note that in Ref. [42] the tight-binding parameters at the interface are modified to fit the experimental value of $V_{\Gamma X}$, while we have used the bulk parameters without any modifications beyond the virtual crystal approximation. Besides, the use of the virtual crystal approximation in our calculations implies that the observed behaviour of $V_{\Gamma X}$ is a consequence of the diffusion-related change of the SL symmetry in z direction, and is not connected to the lateral disorder at the interfaces. As pointed out in [42], in the presence of lateral steps at the interfaces (which is often the case in AlAs/GaAs heterostructures) the experimentally observed value of $V_{\Gamma X}$ should be the average between the four possible even/odd configurations for (m, n). Our results show that $V_{\Gamma X}$ is identically zero for odd values of m, and decreases rapidly with increasing L_D for even m. Therefore, the averaged $\Gamma{-}X$ coupling should depend strongly on the degree of intermixing, thus providing a direct measure for the interface alloying in the SL.

3.3. SUPERLATTICES CONTAINING EMBEDDED WELLS WITH GRADED INTERFACES

3.3.1. Investigated nanostructures

We consider an 18 ML thick GaAs quantum well, embedded in an $(AlAs)_4$/ $(GaAs)_8$ SL. The SL has 5.5 periods (five wells and six barriers) on each side of the EW and is surrounded by semi-infinite $Al_{0.33}Ga_{0.67}As$ barriers. The growth direction is [001]. For comparison two 18 ML thick $Al_xGa_{1-x}As$ /GaAs single quantum wells (SQWs) are considered. The first one (SQW1) has $x = 1$ and

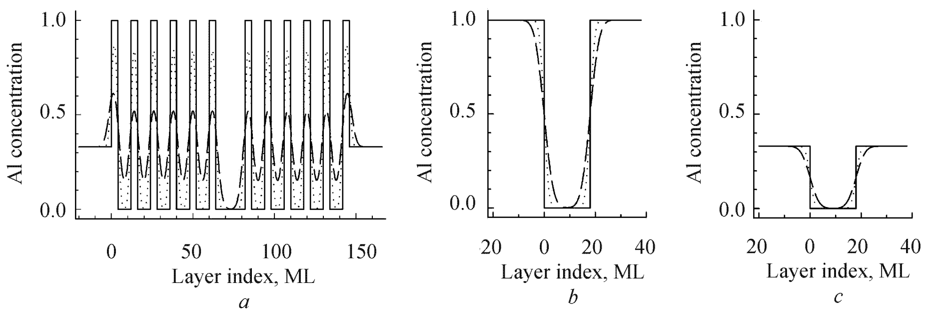

Fig. 12. Concentration profiles of the EW (a), SQW1 (b), and SQW2 (c) for nondiffused (solid line) and diffused structures with $L_D = 2$ ML (dotted curves) and $L_D = 4$ ML (dashed curves)

the second one (SQW2) $x = 0.33$ equal to the mean Al content in the SL. The interface grading is described using the model depicted in Sect. 3.1. The diffusion length is used as a parameter characterizing the degree of interface broadening. The calculations are made for L_D values between 0 and 4 ML in steps of 0.1 ML. The concentration profile of the structure is obtained by means of formula (2). (see Sect. 3.1). The obtained Al concentration profiles of the EW, SQW1 and SQW2 for $L_D = 0, 2$ and 4 ML are given in Fig.12.

3.3.2. Envelope function approximation

The bound state energies at the Γ point of the 2D Brillouin zone are calculated in frames of the one-band EFA model. The calculation procedure and the parameters used are the same as in Sect. 2.2. and 3.2.1., but now the grading of the interface potential and the SL perturbation by the EW are taken into account. The calculated energies of the lowest electron (E), HH and LH bound states of the EW are plotted in Fig. 13.

The lowest bound states E1, HH1 and LH1 originate from the embedded well [44] and their behaviour is qualitatively the same as in an SQW (see [20] and

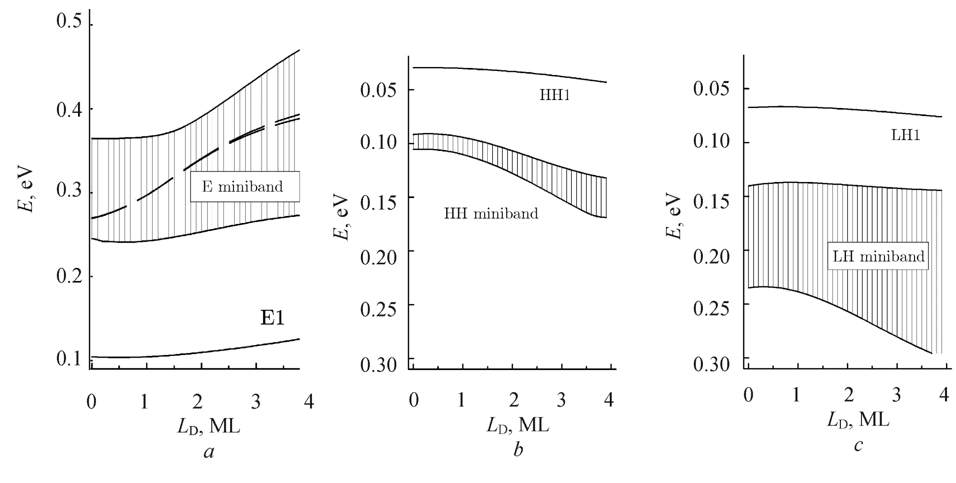

Fig. 13. Energies of bound states versus L_D in the EW: *a*) electrons, *b*) heavy holes, and *c*) light holes. The energies of the conduction band bound states originating from the X points of the Brillouin zone are shown with dashed curves in (*a*). The calculations are performed by means of the EFA

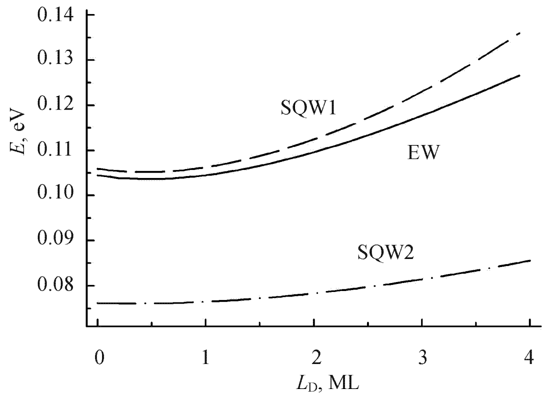

Fig. 14. Energy of the first electron bound state E1 versus the diffusion length L_D in the EW (solid curve), SQW1 (dashed curve) and SQW2 (dash-dotted curve). The calculations are performed by means of the EFA

Fig. 14): the states move further from the band edges as L_D increases. As in the SQW, here we have two competing effects [20]. First, the decrease of the potential in the barrier regions pushes the bound state energies closer to the band edges; and second, the increase of the potential in the embedded well region pushes the energies further from the band edges. As the lowest bound state wavefunctions are localized mainly in the embedded well region, they are more sensitive to the change of the potential inside the well than outside it. This implies that the second effect prevails and we observe an increase of the energies with L_D.

The weak extrema in the energies at $L_D = 0.5$ ML, observed in Fig. 13 and more clearly in Figs. 14 and 15 are due to the quadratic dependence of E_G on the Al mole fraction (see Sec. 2.2). For lower Al concentrations in the barrier regions ($x < 0.4$) this dependence is often assumed linear [45], and in such cases the bound state energy extrema appear at $L_D = 0$ (i.e., abrupt interfaces).

A comparison between the state E1 and the first electron states in SQW1 and SQW2 is presented in Fig. 14. The SQW2 state has significantly lower energy than E1 in the EW because of the lower barriers of SQW2. The energy change of this state with L_D is also smaller. This is due to the fact that at small diffusion lengths there is more AlAs diffusing in the EW (from the nearest AlAs layers) than in SQW2. Therefore, the potential in the EW changes more rapidly with diffusion and the E1 state exhibits larger energy shift compared to SQW2.

The E1 states in EW and SQW1 are close in energy and show similar behaviour. The energy difference between them increases with L_D and reaches 10 meV for $L_D = 4$ ML. The reason for this difference is that the barriers in the EW are thin and the potential in the barrier regions decreases more rapidly with diffusion than in SQW1. Therefore stronger compensation of the two above-discussed energy shifts occurs and E1 is less sensitive to diffusion in the EW than in SQW1. The same holds also for the LH1 and HH1 states.

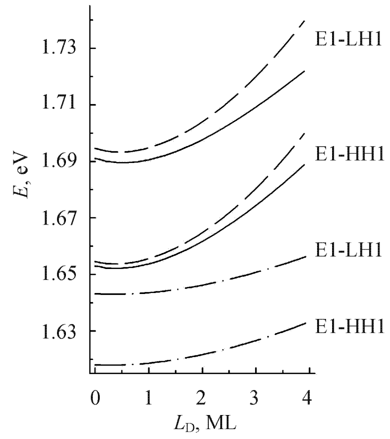

Fig. 15. Transition energies versus the diffusion length L_D in the EW (solid curve), SQW1 (dashed curve) and SQW2 (dash–dotted curve) for the transitions (E1–HH1) and (E1–LH1), calculated by means of the EFA

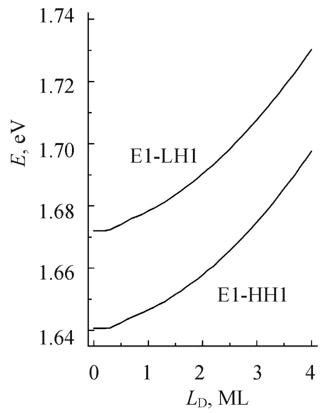

Fig. 16. Transition energies versus the diffusion length L_D in the EW for the transitions (E1–HH1) and (E1–LH1), calculated by the empirical tight-binding method

The transition energy dependencies on the diffusion length L_D for the transitions (E1–HH1) and (E1–LH1) in the EW, SQW1 and SQW2 are plotted in Fig. 15. A blue shift is observed for all transitions as L_D increases. The maximum shift (at $L_D = 4$ ML) for the transition (E1–HH1) is 37 meV in the EW, 48 meV in SQW1 and 15 meV in SQW2 and for (E1–LH1)—32, 48 and 14 meV respectively. This shift is greater in SQW1 than in the EW, and is significantly smaller in SQW2, in accordance with the behaviour of the corresponding states.

3.3.3. Empirical tight-binding method

The calculated transition energies between the lowest states of the EW are shown on Fig.16. They differ only qualitatively from those, obtained by the EFA. Because a linear dependence of E_G on the Al mole fraction is used here, the energy minimum occurs at $L_D = 0$ ML (sharp interfaces). The blue shift at $L_D = 4$ ML is higher than the one calculated by the EFA and is equal to 57 and 58 meV for E1–HH and E1–LH transitions, respectively.

4. CONCLUSION

We have performed a detailed theoretical and computer simulation study of the electronic structure of AlAs/GaAs SLs, containing one centred GaAs EW with abrupt and graded interfaces. The calculations are carried our by means of the EFA and the ETB methods. The behaviour of the electron and hole bound states for a wide range of EW widths (from 2 to 50 MLs) is studied for the case of abrupt interfaces. Emphasise is given on the interaction between EW and SL states. This interaction occurs when an EW state is close in energy or inside a SL miniband and holds only for states of equal parity. It is manifested by energy shifts and substantial changes in the wavefunction localization of the interacting states: the EW state delocalizes towards the SL and SL states penetrate in the EW. The application of the ETB approach allows obtaining interesting features of the electronic structure, which are inaccessible for the simple EFA model.

The theoretical analysis is extended towards real interfaces by considering non-abrupt interface profiles, which are due to the material intermixing at the interfaces. The non-abrupt interfaces are modelled by a concentration profile, obtained by solving the diffusion equation, the diffusion length being a measure of the interface broadening. The model is applied first to regular $(AlAs)_m/(GaAs)_n$ SLs with graded interfaces. It is demonstrated that increasing the degree of interface grading has two important consequences. First, a transformation from type I (direct) SL to type II (indirect) SL is possible. The critical diffusion length, above which this transition occurs, is smaller for smaller n and larger m. The essential changes of the SL properties accompanying such a transition give new opportunities for various applications of the described phenomenon. Second, the Γ−X coupling in the SL conduction band decreases rapidly when m is even, while for odd m it is identically zero. The magnitude of the coupling matrix element can therefore be used as a very sensitive probe of the interface quality in SLs.

This result could explain the difficulties arising in attempts to demonstrate experimentally the dependence of the Γ−X mixing on the parity of m, because some intermixing at the interfaces always takes place in real heterostructures.

Finally the influence of the interface broadening on the electronic structure and the optical transition energies is investigated in $(AlAs)_4/(GaAs)_8$ SLs with one EW of 18 MLs. The behaviour is similar to that observed in a single QW with AlAs barriers, but the transition and states energies are less sensitive to diffusion in the EW, because in this case the barrier potential decreases more rapidly. The minibands of the superlattice are also affected by the interface broadening. They get wider and move away from the band edges as L_D increases. The proposed model of interface broadening can also be applied to study purposely-annealed semiconductor multilayers.

ACKNOWLEDGEMENTS

Financial support from the Bulgarian National Science Fund and the Sofia University Research Fund is acknowledged. The authors are grateful to Prof. V. R. Velasco and to B. Hristov for helpful discussions. Thanks are due to M. Saraydarov for technical help.

REFERENCES

1. Smith, S. D. Optoelectronic Devices, Prentice Hall, London, 1995.
2. Weisbuch, C. , and B. Winter. Quantum Well Structures. Fundamentals and Applications, Academic Press, New York, 1991.
3. Bastard, G. Wave Mechanics Applied to Semiconductor Heterostructures, Les Editions de Physique, Les Ulis, 1988.
4. Steslicka, M., R. Kucharczyk, A. Akjouj, B. Djafari-Rouhani, L. Dobrzynski, and S. G. Davison. *Surf. Sci. Rep.*, **47**, 2002, 93.
5. Kucharczyk, R. , and M. Steslicka. *Sol. St. Com.*, **81**, 1992, 557.
6. Arriaga, J., and V. R. Velasco. *J. Phys.*: Condensed Matter, **7**, 1995, 3493.
7. Blood, P. In: Physics and Technology of Heterojunction Devices, eds. D. V. Morgan, and R. H. Williams , Peter Perigrinus, London, 1991, p. 231.
8. Sakaki, H., M. Tsuchiya, J. Yshino. *Appl. Phys. Lett.*, **47**, 1985, 295.
9. Kapon, E., G. Biasiol, D.M. Hwang, M. Walther, E. Colas. *Sol. St. Com.*, **40**, 1996, 815.
10. Shtinkov, N., V. Donchev, K. Germanova, H. Kolev. *Semicond. Sci. Technol.*, **15**, 2000, 946.
11. Shtinkov, N., S. Vlaev, V. Donchev, K. Germanova. *Phys. Stat. Sol. (b)*, **220**, 2000, 153.
12. Donchev, V., K. Germanova. *Proc. Suppl. Balkan Phys. Lett.*, **5**, 1997, 410.
13. Shtinkov, N.,V. Donchev, and K. Germanova, In: *Thin Films Materials and Devices – Development in Science and Technology*, Eds. J. M. Marshal, N. Kirov, A. Vavrek, and J. M. Maud, World Scientific, Singapore, 1999, 305.
14. Shtinkov, N., V. Donchev, K. Germanova, S. Vlaev, I. Ivanov. *Vacuum*, **58**, 2000, 561.
15. Donchev, V., K. Germanova, N. Shtinkov, I. Ivanov, S. Vlaev. *Thin Sol. Films*, **364**, 2000, 224.
16. Donchev, V., Tzv. Ivanov, I. Ivanov, M. Angelov, K. Germanova. *Vacuum*, **58**, 2000, 478.
17. Donchev, V.,N. Shtinkov, K. Germanova, I. Ivanov, H. Brachkov, Tzv. Ivanov. *Mat. Sci. Engin. C*, **15**, 2001, 75.
18. Deveaud, B., J. Shah, T.C. Damen, B. Lambert, A. Chomette, A.Regreny. *IEEE J. Quan. El.*, **24**, 1988, 1641.
19. Harrison, I. *Semicond. Sci. Technol.*, **9**, 1994, 2053.
20. Vlaev, S., D.A. Contreras-Solorio. *J. Appl. Phys.*, **82**, 1997, 3853.
21. Oh, Y.T., T.W. Kang, T.W. Kim. *J. Appl. Phys.*, **78**, 1995, 3376.
22. Data in Science and Technology. Semiconductors: Group IV Elements and III–V Compounds, Madelung, O. (Ed), Berlin: Springer, 1991.
23. Kopf, R. F., M. H. Herman, M. L. Schoes, and C. Colvard. *J.Vac.Sci.Technol., B*, **11**, 1993, 813.
24 Ky, N. H., J. D. Ganiere, M. Gailhanou, F. Morier-Genaud, D. Martin, and F. K. Reinhart. *Phys. Rev. B*, **46**, 1992, 6947.
25. Luttinger, J. M., and W. Kohn. *Phys. Rev.*, **97**, 1955, 869.
26. Bingelli, N., and A. Baldereschi. *Phys. Rev. B*, **43**, 1991, 14734.
27. Fernandez-Alvarez, L., G. Monsivais, S. Vlaev, and V. R. Velasco. *Surf. Sci.*, **369**, 1996, 367.
28. Vogl, P., H. P. H. Hjalmarson, and J. D. Dow. *J. Phys. Chem. Sol.*, **44**, 1983, 365.
29. Chadi, D. J. *Phys. Rev. B*, **16**, 1977, 790.
30. Kireev, P.S. Semiconductor Physics, Visshaya Shkola, Moscow, 1969, 123 (in Russian)
31. Ourmazd, A., M. Scheffler, M. Heinemann, J-L. Rouviere. *Mater. Res. Bul.*, **27**, 1992, 24.
32. Ourmazd, A., D.W.Taylor, J.Cunningham, and C.W. Tu. *Phys. Rev. Lett.*, **62**, 1989, 933.
33. Warwick, C. A., and R. F. Kopf.. *Appl. Phys. Lett.*,**60**, 1992, 386.
34. Braun, W., A.Trampert, L.Daweritz, K.H.Ploog, *Phys. Rev. B*, **55**, 1997, 1689.
35. Dargam, T.G., and B. Koiller. *Sol. St. Com.*, **105**, 1998, 211.
36. Koiller, B., A. S. Martins, and H. Chacham. *Appl.Phys.Lett.*, **69**, 1996, 2423.
37. Muñoz, M. C., V. R. Velasco, and F. Garcia-Moliner. *Phys. Rev. B*, **39**, 1989, 1786.
38. Vlaev, S., V. R. Velasco, and F. Garcia-Moliner. *Phys. Rev. B*, **49**, 1994, 11222.
39. Ghisoni, M., R. Murray, A. W. Rivers, M. Pate, G. Hill, K. Woodbridge, and G.Parry. *Semicond. Sci. Technol.*, **8**, 1993, 1791.

40. Meynadier, M.-H., R. E. Nahory, J. M. Worlock, M. C. Tamargo, J.-L. de Miguel, and M. D. Sturge. *Phys. Rev. Lett.*, **60**, 1988, 1338.
41. Wang, L.-W., A. Franceschetti, and A. Zunger. *Phys. Rev. Lett.*, **78**, 1997, 2819.
42. Menchero, J. G., B. Koiller, and R. B. Capaz. *Phys. Rev. Lett.*, **83**, 1999, 2034.
43. Lu, Y. T., and L. J. Sham. *Phys. Rev. B*, **40**, 1989, 5567.
44. Donchev, V., Tzv. Ivanov, and K. Germanova. In: *Advanced Electronic Technologies and Systems Based on Low-Dimensional Quantum Devices*, Ed. M.Balkanski, Kluwer, Dordrecht, 1997, 51.
45. Seidel, W., and P. Voisin. *Semicond. Sci. Technol.*, **8**, 1993, 1885.

Received April 2004

Vesselin Donchev
St. Kliment Ohridsi University of Sofia
Faculty of Physics
Department of Condensed Matter Physics
5 J. Bourchier Blvd.
BG-1164 Sofia, Bulgaria
E-mail: vtd@phys.uni-sofia.bg